THE JOURNAL OF PHYSICAL CHEMISTRY A

Article

pubs.acs.org/JPCA

Positional Isotope Exchange in $HX\cdot(H_2O)_n$ (X = F, I) Clusters at Low Temperatures

Yair E. Litman,[†] Pablo E. Videla,[†] Javier Rodriguez,[‡,¶] and Daniel Laria*[,†,‡]

[†]Departamento de Química Inorgánica, Analítica y Química-Física and INQUIMAE-CONICET, Facultad de Ciencias Exactas y Naturales, Universidad de Buenos Aires Ciudad Universitaria, Pabellón II, 1428 Buenos Aires, Argentina

[‡]Departamento de Física de la Materia Condensada, Comisión Nacional de Energía Atómica, Avenida Libertador 8250, 1429 Buenos Aires, Argentina

[¶]ECyT, UNSAM, Martín de Irigoyen 3100, 1650 San Martín, Pcia. de Buenos Aires, Argentina

ABSTRACT: We present molecular dynamics simulation results describing proton/deuteron exchange equilibria along hydrogen bonds at the vicinity of HX acids (X = F, I) in aqueous clusters at low temperatures. To allow for an adequate description of proton transfer processes, our simulation scheme resorted on the implementation of a multistate empirical valence bond hamiltonian coupled to a path integral scheme to account for effects derived from nuclear quantum fluctuations. We focused attention on clusters comprising a number of water molecules close to the threshold values necessary to stabilize contact-ion-pairs. For X = F, our results reveal a clear propensity of the heavy isotope to lie at the bond bridging the halide to the nearest water molecule. Contrasting, for X = I, the thermodynamic stability is reversed and the former connectivity is preferentially articulated via the light isotope. These trends remain valid for undissociated and ionic descriptions of the stable valence bond states. The preferences are rationalized in terms of differences in the quantum kinetic energies of the isotopes which, in turn, reflect the extent of the local spatial confinements prevailing along the different hydrogen bonds in the clusters. In most cases, these features are also clearly reflected in the characteristics of the corresponding stretching bands of the simulated infrared spectra. This opens interesting possibilities to gauge the extent of the isotopic thermodynamic stabilizations and the strengths of the different hydrogen bonds by following the magnitudes and shifts of the spectral signals in temperature-controlled experiments, performed on mixed clusters combining H_2O and HOD.

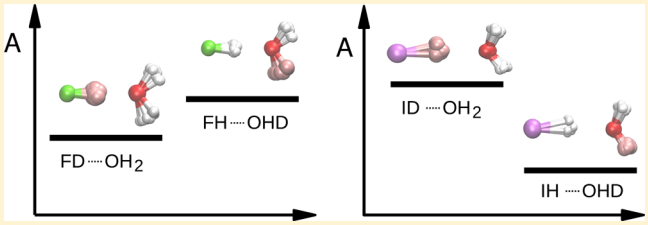

I. INTRODUCTION

Chemical reactivity in clusters differs in a sensible fashion from what is normally perceived in more conventional, bulk environments. For aggregates with linear dimensions in the nanometer range, the causes of such differences are normally ascribed to the presence of a free surface in the close vicinity of most of the cluster constituents. These interfaces introduce strong gradients in the different interparticle force fields that clearly modify key properties describing the reactive processes, such as equilibrium and rate constants, to cite two relevant examples.[1−5]

In aqueous aggregates, microscopic interpretations of the later phenomena normally rely on the examination of the local characteristics of the hydrogen bond topology as a controlling agent of the reactive processes. The examination of water nanoclusters comprising up to, say, ∼10−15 molecules, at temperatures of the order of $T \sim 25-50$ K, is particularly enlightening since the stable conformers usually exhibit solidlike structures with well-defined geometries. This allows for direct characterizations of the hydrogen bonds along the cluster network, which are normally interpreted in terms of the donor/acceptor characters of each component.

The consideration of mixed clusters that incorporate ionic solutes, in turn, opens interesting and new scenarios, most notably in the closest solvation shells of the solutes. For example, by performing a series of mass-selected, spectroscopic experiments, Johnson and collaborators[6−8] were able to elegantly unravel the gradual modifications operated in the hydrogen bond connectivity and in the structure of $H^+(H_2O)_n$ clusters, starting from the resonant Zundel, $[H_2O\cdot H\cdot OH_2]^+$ moiety, up to cluster sizes comprising ∼30 water molecules.[9,10] In a wider context, theoretical[11,12] and direct experiments[13−18] have also been conducted to examine, in systematic fashions, the modifications in the infrared signals that might indicate changes in the solvation structures and intermolecular connectivities prevailing in $X^-\cdot(H_2O)_n$ (X = F, Cl, Br, I) clusters.

Isotopic positional exchange equilibria represents a complementary route to gain additional insights about hydrogen bond strengths and their influence in the solvation structures in the bulk and in clusters.[19] Very recently, we analyzed the

Received: July 4, 2016
Revised: August 16, 2016
Published: August 17, 2016

DOI: 10.1021/acs.jpca.6b06681
J. Phys. Chem. A 2016, 120, 7213−7224

propensities of H and D isotopes to lie at dangling sites, in contraposition with connecting positions, in the water octamer using a path-integral (PI) approach.[20] We found that the differences between the thermodynamic stabilities of the two isotopomers could be traced back to modifications in the quantum spatial delocalization prevailing along perpendicular directions with respect to the relevant O−H intramolecular bonds. Similar equilibria were also examined for the cases of protonated clusters,[21,22] mixed aggregates combining water/halides,[23,24] Zundel moieties "decorated" with noble gas terminal groups,[25] and ionic solvation in bulk water at ambient conditions.[26] Following a similar spirit, in the present work we extend these previous studies and present results for isotopic equilibria extracted from computer simulations that shed light on the characteristics of hydrogen bonding in the close vicinity of hydrogen halides embedded in water clusters. More specifically, we concentrated in aggregates with a number of constituents close to the necessary one for the onset of acid dissociation. In these aggregates, we investigated stable configurations with similar geometrical characteristics, corresponding to undissociated and contact-ion-pair (CIP) states. To do so, we complemented our original PI approach with the incorporation of an empirical valence bond Hamiltonian[27] which allows for adequate descriptions of proton transfer equilibria.

Bibliographic records dealing with the hydration and dissociation mechanisms of H−X acids in water clusters are numerous.[28] Given their relevance in atmospheric chemistry, $HCl\cdot(H_2O)_n$ aggregates have attracted the greatest attention from both, theoretical[29−35] and experimental[36−39] perspectives. Here, instead, given the well-known disparity of the acidic characteristics of the different hydrogen halides in water at ambient conditions (we remark that in passing from HF to HI the corresponding pK_a's differ by ∼13 units), we focused attention on these two limiting cases, namely X = F and I, as prototypes for cluster solvation scenarios of well differentiated weak and strong acids.

The organization of this paper is as follows: in section II, we present details about the model and the simulation procedure. The first part of section III includes results for the structure and energetics of the different clusters. The middle part contains a thermodynamic analysis of isotopic equilibria, whereas in the last part, we present our predictions for the characteristics of the infrared spectra of undissociated and dissociated clusters. Finally, in section IV we summarize the most important conclusions of the work.

II. MODEL AND SIMULATION PROCEDURE

Our simulation strategy was based on a mixed scheme that combines the ring polymer molecular dynamics (RPMD) approximation[40,41] implemented within the PI formulation of quantum statistical mechanics,[42] along with a multistate empirical valence bond (MEVB) model.[27] The latter approach has been successfully implemented in simulation studies of proton transfer processes in a wide variety of aqueous environments.[43−48] On the other hand, the RPMD scheme has also proved to be an adequate simulation route to gauge effects derived from the explicit incorporation of nuclear quantum fluctuations in simulations describing equilibrium and dynamical characteristics of small aqueous clusters.[20,24,49] In what follows, we will briefly highlight the main features of these two complementary methodologies and refer the interested reader to more comprehensive descriptions.[41,43,47]

Empirical Valence Bond Hamiltonian. The basic ingredient of the MEVB methodology relies on the consideration of a Hamiltonian of the type:

$$\hat{H}_{EVB} = \sum_{ii'}^{N_{EVB}} |\phi_i\rangle h_{ii'}(\{\mathbf{r}_N\})\langle\phi_{i'}| \tag{1}$$

where $\{|\phi_i\rangle\}$ represents a basis set of diabatic valence bond (VB) states (i = 1, 2, ..., N_{EVB}) that describe different spatial localizations of a tagged proton. In analyses of acid dissociation equilibria, two types of VB states are normally considered:[44−46,48] (i) on the one hand, a VB state associated with the covalent, undissociated acid (hereafter identified as $|XH\rangle$), and (ii) on the other, a set of dissociated or ionic states of the type $|X^-H^+\rangle$ corresponding to halide-hydronium-ion-pairs, in which the dissociated proton is localized in a water molecule at the close vicinity of the halide. The criterion to determine which VB states are to be included in the construction of the $\hat{H}_{EVB}$ matrix is normally guided by establishing a pattern of a HB network.

The functional forms implemented here in the parametrization of the different matrix elements $h_{ii'}(\mathbf{r})$ follow closely the ones adopted in several previous MEVB studies.[44−46,48,50] In particular, following ref 48, the diagonal matrix element for the covalent diabatic state was parametrized as

$$\langle XH|\hat{H}_{EVB}|XH\rangle = U^{XH} + U^{H_2O} + U^{XH/H_2O} \tag{2}$$

The first term on the right-hand side of the previous equation corresponds to the intramolecular contribution in the acid and was described by a Morse term:

$$U^{XH} = D_{XH}[1 - \exp[-\alpha(r_{XH} - r^{eq})]]^2 \tag{3}$$

The second term includes intra- and intermolecular contributions to the water potential energy and were modeled according to the anharmonic aSPC/Fw force field described in ref 51. The last term represents acid/water interactions and was considered of the form:

$$U^{XH/H_2O} = U^{LJ}_{XO_w} + U^{coul}_{XH-H_2O} + U^{rep}_{XO_w} + U^{rep}_{H_XO_w} \tag{4}$$

In the previous equation, $U^{LJ}_{XO_w}$ and $U^{coul}_{XH-H_2O}$ represent the standard sum of pairwise, site−site, Lennard-Jones plus Coulomb contributions to the acid-solvent interactions, parametrized by implementing the usual arithmetic and geometric means for length and energy parameters, respectively. The last two terms in eq 4 represent additional exponential repulsive contributions of the type:[48]

$$U^{rep}_{XO_w} = B^0 \exp[-b^0(r_{XO_w} - d^0_{XO_w})] \tag{5a}$$

$$U^{rep}_{H_XO_w} = C^0 \exp[-c^0(r_{H_XO} - d^0_{H_XO_w})] \tag{5b}$$

where H_X refers to the H site in the undissociated acid.

The functional form of the diagonal elements for the ionic states comprised the following contributions:

$$\langle X^-H^+|\hat{H}|X^-H^+\rangle = U^{H_3O^+} + U^{H_3O^+/H_2O} + U^{X^-/H_2O} + U^{X^-/H_3O^+} + U^{H_2O} + V_c \tag{6}$$

The first two terms at the right-hand side correspond to intramolecular interactions in the hydronium state and to hydronium/water intermolecular interactions, and they were taken from the aMS-EVB3 model developed by Park and

DOI: 10.1021/acs.jpca.6b06681
J. Phys. Chem. A 2016, 120, 7213−7224

Paesani.[51] The following contributions, U^{X^-/H_3O^+} and U^{X^-/H_2O}, represent intermolecular interactions between the halide X^- and H_3O^+ and the water molecules, respectively, and were modeled according to

$$U^{X^-/H_2O} = U^{LJ}_{X^-/O_w} + U^{coul}_{X^-/O_w} + U^{coul}_{X^-/H_w} \quad (7)$$

and

$$U^{X^-/H_3O^+} = U^{LJ}_{X^-/H_3O^+} + U^{coul}_{X^-/H_3O^+} + U^{rep}_{X^-/O} + U^{rep}_{X^-/H} \quad (8)$$

The repulsive terms in the last equation were of the form:

$$U^{rep}_{X^-/O} = B^{00} \exp[-b^{00}(r_{XO} - d^{00}_{XO})] \quad (9)$$

and

$$U^{rep}_{X^-/H} = C^{00} \exp[-c^{00}(r_{XH} - d^{00}_{XH})] \quad (10)$$

The constant V_c accounts for differences in the energies of the asymptotic states of the two different types of diagonal elements, at large intermolecular distances. Finally, we remark that for clusters involving HI or I^- species, we found it necessary to supplement the previous expressions with a polarization term of the form:

$$V_{pol} = \frac{1}{2}\alpha_I \mathbf{E}^2 - \boldsymbol{\mu}_I \cdot \mathbf{E} \quad (11)$$

with

$$\boldsymbol{\mu}_I = \alpha_I \mathbf{E} \quad (12)$$

where $\boldsymbol{\mu}_I$ is the induced dipole, α_I the polarizability, and $\mathbf{E}$ represents the external Coulomb electric field acting on the halogen and the acid. Additional polarization contributions in the force fields involving solvent species, beyond the incorporation of flexibility in the positions of the nuclei, were not considered. The latter is an approximation that would otherwise be debatable in discussions involving "surface" versus "bulk" ionic solvation in much larger, liquidlike, aqueous clusters,[52−56] which do not seem relevant in the present analysis.

The expression of nondiagonal elements that couple diabatic states localized at adjacent water molecules were also taken from ref 51. The parametrization of off-diagonal matrix elements of the type $\langle X^-H^+|\hat{H}_{EVB}|XH\rangle$ were approximated from the usual form:[44−46,48]

$$\langle X^-H^+|\hat{H}_{EVB}|XH\rangle = V_{const} A(r_{XO}, q) \quad (13)$$

where

$$A(r_{XO}, q) = \exp(-\gamma q^2)[0.5 - \tanh[\beta(r_{XO} - r^0)]] \quad (14)$$

and

$$q = r_{XH,XO} - \frac{r_{XO}}{2}\left(r^0_{sc} - \frac{r_{XO} - \tilde{r}}{15\text{Å}}\right) \quad (15)$$

In the previous equation, $r_{XH,XO} = \hat{\mathbf{r}}_{XO} \cdot \mathbf{r}_{XH}$ represents the projected distance between X and the resonant proton along the direction described by the unit vector $\hat{\mathbf{r}}_{XO}$.

In Table 1, we list the set of parameters that were optimized in order to bring energy predictions from the EVB Hamiltonian in reasonable agreement with results obtained from quantum calculations. The procedure involved the implementation of the SIMPLEX algorithm, following the procedure described in ref 45, taking as a reference quantum results of dissociative curves for isolated dimers at a set of relevant, fixed X−O distances.

Table 1. Parametrization of the $\hat{H}_{EVB}$

X		F	I
D_{XH}	(kcal mol^{-1})	135.0	105.0
α	(Å^{-1})	2.26	1.50
r^{eq}	(Å)	0.917	1.609
σ_{X/O_w}	(Å)	3.10	3.547
ϵ_{X/O_w}	(kcal mol^{-1})	0.184	0.30
q_H (HX)	(e)	0.567	0.15
q_X (HX)	(e)	−0.567	−0.15
B^0	(kcal mol^{-1})	1.00	1.40
b^0	(Å^{-1})	0.55	3.00
$d^0_{XO_w}$	(Å)	2.5	3.7
C^0	(kcal mol^{-1})	3.80	20.0
c^0	(Å^{-1})	10.0	13.0
$d^0_{H_3O_w}$	(Å)	1.25	1.15
σ_{X^-/O_w}	(Å)	3.142	4.168
ϵ_{X^-/O_w}	(kcal mol^{-1})	0.0974	0.1247
σ_{X^-/H_3O^+}	(Å)	3.05	4.168
ϵ_{X^-/H_3O^+}	(kcal mol^{-1})	0.1324	0.1247
q_{X^-}	(e)	−1	−1
B^{00}	(kcal mol^{-1})	6.49	2.00
b^{00}	(Å^{-1})	5.46	2.00
d^{00}_{XO}	(Å)	2.3	3.7
C^{00}	(kcal mol^{-1})	5.00	4.84
c^{00}	(Å^{-1})	7.50	10.0
d^{00}_{XH}	(Å)	1.25	1.95
V_c	(kcal mol^{-1})	195.0	147.0
V_{const}	(kcal mol^{-1})	−15.79	−30.49
γ	(Å^{-2})	1.13	1.39
β	(Å^{-1})	4.60	0.785
r^0	(Å)	3.17	4.02
r^0_{sc}		1.40	1.68
$\tilde{r}$	(Å)	1.06	0.682
α_{HI}	(Å^3)		5.41[a]
α_{I^-}	(Å^3)		7.43[b]

[a]From ref 59. [b]From ref 60.

These results corresponded to minimum energy calculations computed at the MP2/aug-cc-pVTZ level of theory and were obtained with the GAUSSIAN-03 package.[57] For computations involving clusters with I species, we employed a consistent aug-cc-pVTZ-PP basis set.[58]

Ring Polymer Molecular Dynamics. As we mentioned previously,[59,60] nuclear quantum effects on equilibrium and dynamical characteristics pertaining to acid dissociation in different clusters were examined by implementing the RPMD approximation, within the PI formalism of quantum statistical mechanics. The starting point of the methodology is the consideration of the standard P-bead discretization of the quantum canonical partition function for the set of N nuclei with coordinates $\{\mathbf{r}_N\}$, at the inverse temperature β, namely:[61]

$$Q_P = \frac{1}{h^{3PN}} \int \cdots \int \prod_{k=1}^{P} \prod_{j=1}^{N} d\mathbf{r}_j^{(k)}\, d\mathbf{p}_j^{(k)}\, e^{-\beta_P H_P(\{\mathbf{p}_j^{(k)}\},\{\mathbf{r}_j^{(k)}\})} \quad (16)$$

where $\beta = (k_B T)^{-1} = P\beta_P$ and

DOI: 10.1021/acs.jpca.6b06681
J. Phys. Chem. A 2016, 120, 7213−7224

$$H_P(\{\mathbf{p}_j^{(k)}\}, \{\mathbf{r}_j^{(k)}\}) = \sum_{j=1}^{N}\sum_{k=1}^{P}\left[\frac{(\mathbf{p}_j^{(k)})^2}{2M_j} + \frac{M_j\omega^2}{2}(\mathbf{r}_j^{(k)} - \mathbf{r}_j^{(k+1)})^2\right] + \sum_{k=1}^{P}\epsilon_0^{(k)}(\mathbf{r}_1^{(k)}, \mathbf{r}_2^{(k)},..., \mathbf{r}_N^{(k)}) \quad (17)$$

In the previous equation, $\omega = (\beta_P\hbar)^{-1}$, whereas $\mathbf{r}_j^{(k)}$ and $\mathbf{p}_j^{(k)}$ represent the position and momentum of the jth particle of mass M_j at the imaginary time slice k, respectively ($\mathbf{r}_j^{(P+1)} = \mathbf{r}_j^{(1)}$).

The connection between the PI and MEVB schemes is established by the incorporation of $\epsilon_0^{(k)}(\{\mathbf{r}_N^{(k)}\})$ in the Boltzmann factor in eq 16. The latter term represents the Born-Openheimer potential energy surface corresponding to the ground state $|\psi_0^{(k)}\rangle$of $\hat{H}_{EVB}$ evaluated at the imaginary time slice k, namely:

$$|\psi_0^{(k)}\rangle = \sum_{i}^{N_{EVB}} c_i^{(k)}|\phi_i^{(k)}\rangle \quad (18)$$

which satisfies:

$$\epsilon_0^{(k)}(\{\mathbf{r}_N^{(k)}\}) = \sum_{ii'}^{N_{EVB}} c_i^{(k)}c_{i'}^{(k)}h_{ii'}(\{\mathbf{r}_N^{(k)}\}) \quad (19)$$

RPMD estimates for quantum thermal averages for position dependent observables $\langle O\rangle_P$ coincide with those obtained in standard PIMD simulations, namely:

$$\langle O\rangle = \frac{1}{Q_P h^{3PN}}\int\cdots\int\prod_{k=1}^{P}\prod_{j=1}^{N}d\mathbf{r}_j^{(k)}\,d\mathbf{p}_j^{(k)}\,e^{-\beta_P H_P}O_P(\{\mathbf{r}_j^P\}) \quad (20)$$

where

$$O_P(\{\mathbf{r}_j^P\}) = \frac{1}{P}\sum_{k=1}^{P}O(\{\mathbf{r}_j^{(k)}\}) \quad (21)$$

Moreover, the RPMD scheme provides reasonable estimates for dynamical quantities via an approximate expression for Kubo-transformed correlation functions $K_{AB}(t)$ for the observables $\mathcal{A}$ and $\mathcal{B}$, namely:[40]

$$C_{AB}^{RPMD}(t) = \langle\mathcal{A}\mathcal{B}(t)\rangle_{RPMD} \sim K_{AB}(t) \quad (22)$$

$$K_{AB}(t) = \frac{1}{\beta Q(\beta)}\int_0^\beta d\lambda\,\mathrm{Tr}[e^{-\beta\hat{H}}\hat{\mathcal{A}}(-i\lambda\hbar)\hat{\mathcal{B}}(t)] \quad (23)$$

where

$$C_{AB}^{RPMD}(t) = \frac{1}{Q_P h^{3PN}}\int\cdots\int\prod_{k=1}^{P}\prod_{j=1}^{N}d\mathbf{r}_j^{(k)}\,d\mathbf{p}_j^{(k)} \times e^{-\beta_P H_P}\mathcal{A}_P(\{\mathbf{r}_j^P(0)\})\mathcal{B}_P(\{\mathbf{r}_j^P(t)\}) \quad (24)$$

In the previous expressions, the time evolution of the set of coordinates $\{\mathbf{r}_j^P(t)\}$ is dictated by the classical Newton's equations of motions which, invoking Hellmann–Feynman's theorem,[62] take the form:

$$M_j\frac{d^2\mathbf{r}_j^{(k)}}{dt^2} = -\sum_{ii'}^{N_{EVB}}c_i^{(k)}c_{i'}^{(k)}\nabla_{\mathbf{r}_j^{(k)}}h_{ii'}(\{\mathbf{r}_N^{(k)}\}) \quad (25)$$

The systems under investigation were nanoclusters of the type $HX\cdot(H_2O)_n$ (X = F, I), at a temperature of T = 25 K. At this thermal regime, the aggregates exhibit solidlike, dynamical characteristics, with no changes in the original intermolecular connectivity and absence of spontaneous evaporation episodes. The number of VB states considered was $N_{EVB} = n + 1$, accounting for descriptions in terms of a covalent configuration of the type $HX\cdot(H_2O)_n$ and a set of ionic states of the type $X^-H_3O^+(H_2O)_{n-1}$, in which proton is considered localized at one tagged water molecule. To integrate the equations of motion of all pseudoparticles we implemented a transformation from Cartesian to normal mode coordinates,[63] coupled to a multiple time step algorithm,[64] discriminating intramolecular modes in the isomorphic polymers from the rest of the components to the total forces.

The number of beads was set to P = 300; we checked that this value was sufficient to guarantee statistical averages within 2−5% uncertainty. For equilibrium properties these averages were computed from canonical trajectories lasting typically 1 ns, in which each component of each normal mode coordinate was coupled to a Langevin thermostat.[65] Averages from time-dependent properties were harvested from 10 statistically independent trajectories lasting 100 ps, whose initial conditions were taken from the previous canonical trajectories.

III. RESULTS

Energetics and Structures of $HX\cdot(H_2O)_n$ Clusters. The starting point of our analysis will be the consideration of dimers of the type $XH^b\cdots OH_2^e$ (X = F, I), where with the superscripts "b" and "e" we will discriminate "bridge" from "external" positions, respectively (see Figure 1a). In Figures 2 and 3, we present results for dissociative curves obtained from MP2 calculations and predictions from the EVB Hamiltonian for isolated dimers, at a set of fixed donor−acceptor distances. For both halogens, the agreement between the two sets of data is

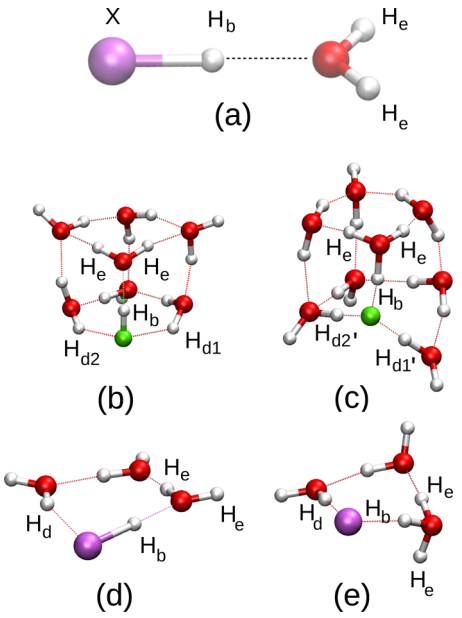

Figure 1. Typical stable configurations for $HX\cdot(H_2O)_n$ clusters. (a) $XH^b\cdots OH_2^e$ dimer; (b) undissociated $FH^b\cdots OH_2^e(H_2O)_6$; (c) dissociated $F^-\cdots(H^bOH_2^e)^+(H_2O)_7$; (d) undissociated $IH^b\cdots OH_2^e(H_2O)_2$; and (e) dissociated $I^-\cdots(H^bOH_2^e)^+(H_2O)_2$. For clarity purposes, F and I atoms are rendered in light green and in mauve, respectively.

DOI: 10.1021/acs.jpca.6b06681
J. Phys. Chem. A 2016, 120, 7213−7224

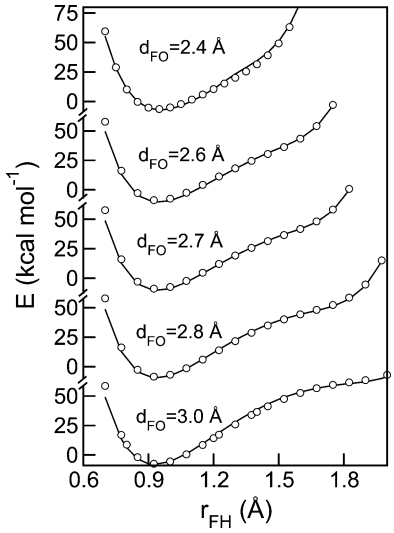

Figure 2. Dissociation energies as a function of the F−H distance, for global minima of the FH···OH_2 dimer, at fixed FO distances. The solid line corresponds to results from the EVB Hamiltonian, whereas the ○ correspond to MP2 results (see text).

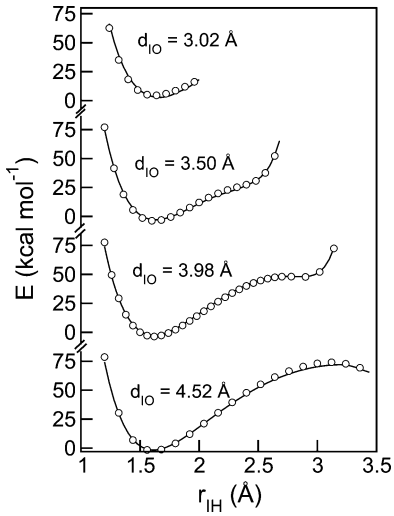

Figure 3. Same as Figure 2 for IH···OH_2.

quite satisfactory; moreover, for the particular case of HF, the quantum plots look comparable to those reported in ref 48. The same can be said about the results for relevant distances and angles for the global minima which are listed in Table 2a. Yet, the direct comparison between interatomic distances in the dimers and in the isolated molecules (shown between parentheses) reveals no meaningful changes and, consequently, does not provide clues to anticipate differences in the acidic characteristics of either halogen.

To proceed, we moved to the examination of clusters comprising a number of water molecules, *n*, close to the values that would stabilize dissociated CIPs. Previous quantum calculations[66−69] have suggested that HF·$(H_2O)_n$ clusters would exhibit stable CIP configurations as *n* reaches ∼8, whereas for HI, that threshold number would drop down to only ∼3 water molecules.[67,70] In Figure 1 (panels b−e), we show typical configurations reported for stable undissociated and dissociated moieties; as such, in what follows, we will use them as benchmarks to analyze isotopic equilibria. Incidentally,

Table 2. Geometrical Parameters for Clusters

	$FH^b \cdots OH_2^e$		$IH^b \cdots OH_2^e$	
a. dimers	EVB[a]	MP2	EVB	MP2
d_{XH^b}	0.94 (0.92)	0.94	1.63(1.61)	1.62
d_{H^eO}	1.0 (1.0)	0.97	1.0 (1.0)	0.97
d_{H^bO}	1.66	1.71	1.94	2.05
θ_{XH^bO}	180.0	178.5	180.0	178.4
b. FH·$(H_2O)_n$ clusters	atom		$\langle d_{FHi}\rangle$	$\langle\theta_{F-Hi-O}\rangle$
FH ··· $OH_2(H_2O)_6$	H_{d1}		2.41 ± 0.28	107 ± 42
	H_{d2}		2.29 ± 0.27	116 ± 40
	H^b		0.97 ± 0.07	167 ± 12
$F^- \cdots H_3O^+(H_2O)_7$	$H_{d1'}$		1.42 ± 0.11	172 ± 8
	$H_{d2'}$		1.38 ± 0.10	172 ± 8
	H^b		1.35 ± 0.10	168 ± 10
c. IH·$(H_2O)_n$ clusters	atom		$\langle d_{IHi}\rangle$	$\langle\theta_{I-Hi-O}\rangle$
IH ··· $OH_2(H_2O)_2$	H^b		1.67 ± 0.09	169 ± 9
	H_d		3.18 ± 0.23	146 ± 29
$I^- \cdots H_3O^+(H_2O)_2$	H^b		1.99 ± 0.11	170 ± 9
	H_d		2.46 ± 11	171 ± 9

[a]EVB values correspond to quenched structures. Quantities between parentheses correspond to isolated molecules. Lengths are expressed in Å; angles are expressed in degrees.

we remark that the undissociated stable structure shown in Figure 1b does not correspond to the actual free energy minimum configuration for the HF·$(H_2O)_7$ cluster which would be characterized by a nonconnected ion pair located at opposite corners of a cubiclike structure.[71] At temperatures of the order of $T \sim 50$ K, the free energy difference between the latter structure and the one shown in Figure 1b is of the order of approximately $-7\ k_BT$. Still, interconversions between them would require surmounting activation free-energy barriers of considerable magnitudes (typically of the order of $\sim 30\ k_BT$), a fact that would support the validity of our analysis of this metastable structure. The overall shapes of both, (b) undissociated and (c) dissociated, clusters can be cast in terms of fairly cubiclike structures where the acid acts as an H-bond donor to a double-donor−single-acceptor water molecule. The larger aggregate, though, exhibits a distorted edge, where an additional single donor water molecule (hereafter labeled *d*1′) attaches along one side of the original structure. Interestingly, a closer look reveals that this geometrical arrangement allows for stronger bindings to the halide of the type OH···F^-, involving the single-donor molecules $H_{d1'}$ and $H_{d2'}$, compared to the connectivity in the undissociated cluster, operated via the double-donor-single-acceptors H_{d1} and H_{d2}. The comparison between a set of relevant distances and angles in the two clusters confirms this observation. In Table 2b, we list quantum averages for the distances d_{FH} and for the angles θ_{F-H-O}, which characterize hydrogen bonding to the halogen in both moieties. For the dissociated cluster, one observes: (i) shorter $H_{di'}$···F distances, (ii) a more marked O−$H_{di'}$···F alignment and, more importantly, (iii) a clear increment in the F − H^b distance.

Previous studies have suggested that the key elements controlling dissociation processes of HF in bulk water[72,73] and in clusters[66,71] are different and, in neither case, they would be directly connected to solute−solvent hydrogen bonding. Contrasting, a more recent analysis concludes that large angular, rather than translational, modifications in the hydrogen-bond architecture are involved upon dissociation in solution.[48] Anyhow, the simple inspection of the modifications

DOI: 10.1021/acs.jpca.6b06681
J. Phys. Chem. A 2016, 120, 7213−7224

Table 3. Free-Energy Differences for Isotopic Positional Exchange and Quantum Kinetic Energies at "Bridge" and "External" Locations in HX ··· $(H_2O)_n$

a. $XD^b \cdots OH_2^e \rightarrow XH^b \cdots OD^eH^e$								
X	ΔA^a	ΔA^b	$\langle T^{\parallel}_{H^b}\rangle$	$\langle T^{\perp}_{H^b}\rangle$	$\langle T^{\parallel}_{H^e}\rangle$	$\langle T^{\perp}_{H^e}\rangle$	$\langle T^{\parallel}_{H^b}\rangle - \langle T^{\parallel}_{H^e}\rangle$	$\langle T^{\perp}_{H^b}\rangle - \langle T^{\perp}_{H^e}\rangle$
F	4.6	4.2	43.6	22.2	41.8	16.9	1.8	5.3
I	−12.2	−12.5	28.7	7.8	41.2	16.7	−12.5	−8.9
b. $XD^b \cdots OH_2^e(H_2O)_n \rightarrow XH^b \cdots OD^eH^e(H_2O)_n$								
X	ΔA^a	ΔA^b	$\langle T^{\parallel}_{H^b}\rangle$	$\langle T^{\perp}_{H^b}\rangle$	$\langle T^{\parallel}_{H^e}\rangle$	$\langle T^{\perp}_{H^e}\rangle$	$\langle T^{\parallel}_{H^b}\rangle - \langle T^{\parallel}_{H^e}\rangle$	$\langle T^{\perp}_{H^b}\rangle - \langle T^{\perp}_{H^e}\rangle$
F	1.07	0.76	40.9	25.2	43.5	21.3	−2.6	3.9
I	−17.0[c]	−17.0[c]	25.5	11.5	42.2[c]	24.0[c]	−16.7[c]	−12.5[c]
	−13.0[d]	−13.1[d]			43.3[d]	16.1[d]	−17.8[d]	−4.6[d]
c. $X^- \cdots (D^bH_2^eO)^+(H_2O)_n \rightarrow X^- \cdots (H^bH^eD^eO)^+(H_2O)_n$								
X	ΔA^a	ΔA^b	$\langle T^{\parallel}_{H^b}\rangle$	$\langle T^{\perp}_{H^b}\rangle$	$\langle T^{\parallel}_{H^e}\rangle$	$\langle T^{\perp}_{H^e}\rangle$	$\langle T^{\parallel}_{H^b}\rangle - \langle T^{\parallel}_{H^e}\rangle$	$\langle T^{\perp}_{H^b}\rangle - \langle T^{\perp}_{H^e}\rangle$
F	1.40	1.49	33.7	37.1	34.9	33.4	−1.2	3.7
I	−6.7[c]	−7.6[c]	18.2	35.6	35.1[c]	31.7[c]	−16.9[c]	3.9[c]
	−4.3[d]	−5.2[d]			43.3[d]	19.4[d]	−25.1[d]	16.2[d]

[a]From eq 27. [b]From eq 31. [c]External connecting site. [d]External dangling site. Energies are expressed in units of β^{-1}. In all cases, the statistical uncertainties in the kinetic energy averages do not surpass 3%.

operated in the distances of the solvation structures reported here indicate that the closer approach of the two donor water molecules $d1'$ and $d2'$ should necessarily benefit solvation of ionic species in detriment of nonionic alternative structures. Moreover, note that values of $\theta_{F-H_{di}-O}$ in the undissociated cluster do not satisfy the criterion normally implemented in computer simulations to identify hydrogen bonding, which sets the lower threshold angle at ∼150°. The reasons for this lower level of atomic alignment along hydrogen bonds may be traced back to the fact that double-donor molecules are subjected to tighter constrains, imposed by the simultaneous preservation of the linearity of two hydrogen bonds. In this context, a description of the intermolecular connectivity in the undissociated cluster expressed in terms of a network of hydrogen bonds would seem to be only marginally satisfied.

As we mentioned previously, only two additional water molecules are necessary to stabilize $I^-\cdots H_3O^+$ contact ion pairs. In fact, the $HI\cdot(H_2O)_3$ aggregate is singular since it exhibits two stable conformers: on the one hand, the covalent $IH\cdots OH_2(H_2O)_2$ and, on the other, the ionic $I^- \cdots H_3O^+(H_2O)_2$ structure as well. Panels (d) and (e) of Figure 1 contain typical snapshots of the two isomers, both with cyclic connectivities. Contrasting with the HF case, in the covalent structure, one of the "external" positions exhibits connected characteristics while the other one remains dangling. The analysis of quenched structures corresponding to the two conformers reveals that the energy of the ionic one, though, is ∼4.5 kcal mol^{-1} lower than the one for the undissociated structure. In fact, in the course of all the trajectories obtained in this work, we did not detect spontaneous interconversions between these two structures indicating that, at temperatures of the order of $T \sim 25-30$ K, such isomerizations would require the passage over activation free-energy barriers well above thermal energies.

In Table 2c, we list quantum averages for geometrical parameters for the covalent and ionic conformers. The most relevant differences are to be found in the intermolecular connectivities established between the I and the two nearest water molecules, via the H_d and H^b sites. In particular, upon dissociation, (i) the atomic $I^-{-}H^d{-}O$ arrangement looks much more colinear. (ii) The $I{-}H_d$ distance contracts from 3.18 Å down to 2.46 Å, whereas (iii) the $I{-}H_b$ distance stretches from the original 1.67 Å up to 1.99 Å, indicating proton dissociation.

Still, one can gauge the extent of dissociation for both acids from a more quantitative perspective by analyzing the magnitude of PI averages of the coefficients $\langle c_i^2\rangle_{PI}$, corresponding to covalent and ionic descriptions of key diabatic states in the dissociated clusters. For $F^-\cdots H_3O^+(H_2O)_7$, these values are $\langle c^2_{HF}\rangle_{PI} = 0.02$ and $\langle c^2_{H_3O^+}\rangle_{PI} = 0.77$, whereas for $I^-\cdots H_3O^+(H_2O)_2$, we found $\langle c^2_{HI}\rangle_{PI} = 0.26$ and $\langle c^2_{H_3O^+}\rangle_{PI} = 0.65$. Note that the latter set of values would indicate that, for the two particular cluster sizes analyzed, the solvation structure prevailing in the HF cluster promotes a higher degree of dissociation compared to the HI case. Contrasting, the role of quantum fluctuations attenuating the extent of proton transfer looks more important in the description of the dissociation process in the latter case: results from classical (i.e., $P = 1$) simulations show practically no modifications in the magnitudes of the corresponding coefficients for the dissociated $F^-\cdots H_3O^+(H_2O)_7$ moiety, whereas in the $I^- \cdots H_3O^+(H_2O)_2$ case, one observes sensible modifications in the classical predictions, namely, $\langle c^2_{HI}\rangle_{clss} = 0.12$ and $\langle c^2_{H_3O^+}\rangle_{clss} = 0.75$. In addition to the usual considerations of zero-point energy and tunneling effects along the proton transfer coordinate, the causes of the latter changes should also be found in the weakening in the quantum description of the $OH_d\cdots I^-$ bonding (see Figure 1e) which, in turn, would hamper acid dissociation.

Isotopic Substitution. We now turn to the analysis of the propensity of H and D to lie at "bridge" and "external" positions. Interconversions in isolated dimers of the type:

$$XD^b \cdots OH_2^e \rightarrow XH^b \cdots OD^eH^e \tag{26}$$

represent the simplest cases, in which "external" locations coincide with dangling positions. The relative stability of reactant and product states in eq 26 can be estimated by computing ΔA, the associated free energy difference via thermodynamic integration procedures:[74]

$$\Delta A = \int_0^1 d\lambda \left\langle \frac{\partial A(\lambda)}{\partial \lambda} \right\rangle_\lambda \tag{27}$$

where λ represents a control parameter characterizing the reversible mass transformations described in eq 26 and $\langle ... \rangle_\lambda$ represents a quantum statistical average taken with the masses

DOI: 10.1021/acs.jpca.6b06681
J. Phys. Chem. A 2016, 120, 7213−7224

set at fixed $\{M_j(\lambda)\}$. The integrand of the previous equation can be readily evaluated using the virial estimate of the quantum kinetic energy, namely:

$$\left\langle \frac{\partial A(\lambda)}{\partial \lambda} \right\rangle_\lambda = -\sum_j \frac{1}{M_j(\lambda)} \frac{\partial M_j(\lambda)}{\partial \lambda} \times \left[\frac{3}{2\beta} + \frac{1}{2P} \sum_{k=1}^{P} \langle (\mathbf{r}_j^{(k)} - \mathbf{r}_j^C) \cdot \nabla_{\mathbf{r}_j^{(k)}} \epsilon_0^{(k)} \rangle_\lambda \right] \tag{28}$$

where $\mathbf{r}_j^C$ is the position of the polymer centroid associated with the jth particle:

$$\mathbf{r}_j^C = \frac{1}{P} \sum_k^P \mathbf{r}_j^{(k)} \tag{29}$$

Following previous calculations the reversible transformation was performed along linear paths:

$$\begin{aligned} M_H(\lambda) &= M_p(1+\lambda) \\ M_D(\lambda) &= M_p(2-\lambda) \end{aligned} \tag{30}$$

where M_p represents the proton mass. At present, there exist different alternatives based on more refined estimators to compute ΔA.[21,22] However, in the present case, we found an adequate convergence for the integrand in eq 28, with a smooth behavior along the complete λ-interval of interest.

The entries in column two of Table 3a reveal that, for X = F, the free-energy difference associated with the previous isotopic exchange is $\beta\Delta A = 4.6$; contrasting, for X = I, the relative stabilities of light and heavy isotopes are reversed, $\beta\Delta A = -12.2$. In order to rationalize the origins of these qualititative changes, it will be instructive to consider the harmonic approximation for ΔA proposed by Ceriotti et al.,[75] which establishes:

$$\Delta A \sim 2[1 - (m_H/m_D)^{1/2}](\langle T_{H^b} \rangle - \langle T_{H^e} \rangle) \tag{31}$$

This approximation was found to be quite accurate to describe isotopic equilibria for a variety of aqueous environments.[24,76−78] Note that the previous expression is particularly appealing since the free-energy difference is exclusively controlled by the difference between the kinetic energies of the light isotope, at "bridge" and "external" positions.

Estimates for ΔA computed from eq 31 are listed in column three of Table 3. In all cases, the results of the approximation reproduce the values computed from eq 27 within an ∼10−15% difference. The average quantum kinetic energies in eq 31, in turn, can be further decomposed into two orthogonal directions: (i) the first one corresponds to parallel contributions $\langle T_i^{\parallel} \rangle$, along the relevant $\mathbf{r}_{OH}^C$ and $\mathbf{r}_{XH}^C$ centroid vectors; (ii) the second one corresponds to a perpendicular projection, defined as $\langle T_i^{\perp} \rangle = \langle T_i \rangle - \langle T_i^{\parallel} \rangle$. We remark that the values of $\langle T_i \rangle$ and the corresponding decompositions provide estimates for the global and projected quantum spatial dispersions, respectively.

The values listed in Table 3a show that, for the FH ··· OH_2 dimer, the kinetic energy of the proton at the "bridge" position clearly surpasses the one registered at dangling locations. Moreover, the proton at the "bridge" bond exhibits tighter spatial localizations along both parallel and perpendicular projections. These differences can be rationalized by examining the combined effects from the intramolecular interactions and the local characteristics of the intermolecular Coulomb coupling. For example, the simple consideration of the stretching frequency in HF, $\omega_{HF} \sim 4150$ cm^{-1}, which is an ∼10% higher than a typical O−H stretching frequency in water, $\omega_{OH} \sim 3700$ cm^{-1}, would anticipate the increment in the quantum kinetic energy along parallel directions. On the other hand, the increment in $\langle T_{H^b}^{\perp} \rangle$ could be ascribed to effects from the intermolecular Coulomb coupling between the undissociated acid and the acceptor water, which clearly increases the more compact the isomorphic polymers. A similar analysis performed on the IH···OH_2 dimer shows opposite trends in both projections. We can think of, at least, two causes to account for these differences: (i) first, the much lower HI intramolecular stretching frequency, $\omega_{HI} \sim 2300$ cm^{-1}, allowing more delocalized configurations of the isomorphic polymer along the parallel direction and (ii) second, the relaxation of colinearity along the I−H···O bond prevailing, otherwise, in the previous F−H···O case. Contrasting with the HF case, the largest difference in the quantum kinetic energies is registered, in this case, along parallel directions. As such, this interplay between the topologies of intra- and intermolecular interactions provide simple geometrical interpretations of origins of the observed differences in the isotopic stabilities in the two dimers. As a digression, the comparison between the relative isotopic stabilization in these two dimers and the one observed in the resonant $[H_2^eO \cdots H^b \cdots OH_2^e]^+$, Zundel cation, exhibiting an even stronger HB, is instructive. In the latter case, a similar PI-MEVB calculation at $T = 50$ K yields $\langle T_{H^b}^{\parallel} \rangle - \langle T_{H^e}^{\parallel} \rangle = -12.6$, whereas $\langle T_{H^b}^{\perp} \rangle - \langle T_{H^e}^{\perp} \rangle = 11.1$ (both values expressed in units of β^{-1}). As such, the stabilization of the light isotope at the "bridge" position in the Zundel cation is the result of a large cancellation between perpendicular and parallel projections of the kinetic energy differences, contrasting with the present, XH···OH_2 dimer cases in which the two projections exhibit equal signs.

Solvation modifies isotopic equilibria, although the global trends observed in ΔA remain similar. In Table 3b, we list results for clusters exhibiting nondissociated species (i.e., FH···$OH_2(H_2O)_6$ and IH···$OH_2(H_2O)_3$. For the former moiety, $\beta\Delta A$ drops down to ∼1, revealing a much less marked stabilization of D at the "bridge" position. Moreover, the approximate harmonic analysis shows that the main causes of this change are to be found in (i) an increment in the kinetic energy along perpendicular directions at "external" positions and (ii) a drop of the parallel component at the "bridge" location, indicative of an incipient dissociation, along with an increment at the external position which, in turn, leads to a change of sign in the $\langle T_{H^b}^{\parallel} \rangle - \langle T_{H^e}^{\parallel} \rangle$ difference. For IH···$OH_2(H_2O)_3$, the more vivid modifications are found along perpendicular directions involving both "externally" connected and "bridge" positions as well. As a result, $\beta\Delta A$ goes down to approximately −17, revealing a solvation-induced, extra stabilization of the light isotope at "bridge" positions.

Compared to the undissociated case, the relative stability of the deuteron at the "bridge" position in $F^-\cdots DOH_2^+(H_2O)_7$ clusters increases by a factor of ∼1.5, expressed in terms of $\beta\Delta A$. For this particular case, one observes comparable increments in the values of $\langle T_{H^i}^{\perp} \rangle$ contrasting with much more dissimilar modifications in $\langle T_{H^i}^{\parallel} \rangle$. Still, contributions from the former projection are the ones that prevail. In contraposition with the previous scenario, free-energy differences between "bridge" and "external" configurations of the light isotope in ionic clusters containing iodide are drastically reduced by a factor of ∼3, compared to the undissociated case.

DOI: 10.1021/acs.jpca.6b06681
J. Phys. Chem. A 2016, 120, 7213−7224

In this case, again, the most dramatic modifications are to be found in changes along perpendicular directions, most notably in the increment of $\langle T^{\perp}_{H^b} \rangle$ by also a factor of ∼3.

Infrared Spectra. We will conclude the present study by examining whether the local characteristics of the different hydrogen bonds analyzed in previous sections might be inferred from the inspection of the stretching signals of the corresponding infrared spectra. In this context, the key magnitude of interest is the spectral density, which is proportional to the Fourier transform of the second derivative of the total dipole−dipole RPMD time correlation function, namely:

$$I(\omega) \propto \int_0^\infty C^{\mathrm{RPMD}}_{\dot{\mu}\dot{\mu}}(t)\cos(\omega t)\, \mathrm{d}t \tag{32}$$

where

$$C^{\mathrm{RPMD}}_{\dot{\mu}\dot{\mu}}(t) = \langle \dot{\boldsymbol{\mu}}(t)\cdot\dot{\boldsymbol{\mu}}(0)\rangle_{\mathrm{RPMD}} \tag{33}$$

Within the EVB framework, the total dipole moment of the cluster is given by

$$\boldsymbol{\mu}(t) = \frac{1}{P}\sum_{k=1}^{P}\sum_{j=1}^{N} q_j^{(k)}(t)\mathbf{r}_j^{(k)}(t) \tag{34}$$

In the previous expression, $q_j^{(k)}(t)$ denotes a weighted sum of partial charges of site j, computed as

$$q_j^{(k)}(t) = \sum_{i=1}^{\mathrm{N_{EVB}}} |c_i^{(k)}(t)|^2 q_j^i \tag{35}$$

where q_j^i represents the partial charge of site j participating in the ith VB state. Time derivatives of the coefficients $c_i^{(k)}$ were evaluated using standard quantum perturbation theory procedures, namely:[79]

$$\dot{c}_i^{(k)} = \sum_{j\neq 0}^{\mathrm{N_{EVB}}} \frac{1}{\epsilon_0^{(k)} - \epsilon_j^{(k)}} \times \Big[\sum_{n=1}^{N} \langle \psi_j^{(k)}|\nabla_{\mathbf{r}_n^{(k)}}\hat{H}_{\mathrm{EVB}}|\psi_0^{(k)}\rangle\cdot\dot{r}_n^{(k)}\Big]\langle\phi_i^{(k)}|\psi_j^{(k)}\rangle \tag{36}$$

In clusters containing HI or I^- species, eq 34 was supplemented with an additional term of the form:

$$\tilde{\boldsymbol{\mu}}_{\mathrm{I}}(t) = \frac{1}{P}\sum_{k=1}^{P}\sum_{i=1}^{\mathrm{N_{EVB}}} |c_i^{(k)}(t)|^2 \boldsymbol{\mu}_{\mathrm{Ii}}^{(k)}(t) \tag{37}$$

where, similarly, $\boldsymbol{\mu}_{\mathrm{Ii}}^{(k)}$ represents the induced dipole moment of the HI/I^- species in the ith VB, evaluated at the kth imaginary time slice. We remark that in order to avoid the presence of spurious signals originated from intrapolymer dynamical modes,[80] we implemented the procedure reported in ref 81 that removes the coupling between Langevin thermostats and centroid degrees of freedom. Anyhow, although this thermostatization methodology is known to introduce broadenings in the spectral lineshapes and may have limitations in its direct implementation for the case of small molecules, the simulated profiles that we obtained still allowed for appropriate discernments of the key features and frequency shifts we are interested in describe.

The two panels of Figure 4 contain results for the stretching bands of $I(\omega)$ for the undissociated $FH\cdots OH_2(H_2O)_6$ cluster (left-hand side) and for the dissociated $F^-\cdots(HOH_2)^+(H_2O)_7$ moiety (right-hand side). In both cases, the curves labeled (a) correspond to fully protonated clusters. For the covalent state, the spectrum presents a wide single band, spanning the 3000−4000 cm^{-1} frequency interval, that includes a two-peak motif. A normal-mode analysis performed on quenched structures, complemented with the inspection of the modifications operated in the spectra following deuteration at selected positions, led us to clear identifications of each signal. The low-frequency one, located at ω = 3380 cm^{-1} (indicated by a dashed arrow), corresponds to motions of the "bridge" proton, whereas the high-frequency one, located at ω = 3600 cm^{-1} and indicated by a solid arrow, corresponds to dynamical modes involving "external" protons. Note that the ordering in the latter frequencies correlates with one registered for $\langle T^{\parallel} \rangle$ in Table 3b. The analysis of curves (b and c), which correspond to isotopomers with deuterations at these two positions, supports the previous correspondence. In both cases, the modifications include sensible reductions in the magnitude of the tagged peak where the isotopic replacement was operated, along with the appearance of new signals at frequencies ω = 2480 cm^{-1} [curve (b)] and ω = 2590 cm^{-1} [curve (c)]. The positions of these new peaks look similar to the ones one would predict from a direct $\sim 0.5^{1/2}$ mass rescaling of each of the missing original frequencies. In passing, we also remark the presence of two shoulders at $\omega \sim$ 3700 cm^{-1} and ∼3400 cm^{-1}, which correspond to additional collective stretching modes involving the rest of the water molecules. In curves (a and c), the first shoulder can still be detected, whereas the latter one is clearly shadowed by the much broaden signal from the "bridge" stretching mode.

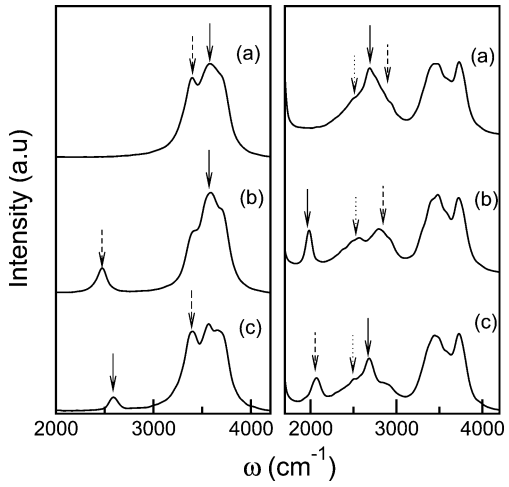

Figure 4. Stretching bands of RPMD infrared spectra of $HF\cdot(H_2O)_n$ clusters. Left panel: undissociated $FH\cdots OH_2(H_2O)_6$; right panel: dissociated $F^-\cdots(HOH_2)^+(H_2O)_7$. The letter code in both panels is the same: (a) fully protonated, (b) isotopomer with deuterium at "bridge" position, and (c) isotopomer with deuterium at "external" position.

A similar analysis performed on the dissociated cluster (right-hand side panel) shows the following features: (i) curve (a) presents a high frequency band, comprising two peaks at ω = 3460 and 3720 cm^{-1}, which correspond to H motions in water molecules not directly connected to the dissociated acid; (ii) in addition, one observes a band with a central signal at ω = 2710 cm^{-1} (indicated by a solid arrow) which corresponds to a dynamical model localized at the "bridge" connective bond in the $(H_3O)^+$ moiety; (iii) the latter signal is flanked by two barely perceptible humps at ω = 2900 cm^{-1} and ω = 2510 cm^{-1}

DOI: 10.1021/acs.jpca.6b06681
J. Phys. Chem. A 2016, 120, 7213−7224

(indicated by dashed and dotted arrows, respectively) which correspond to stretching motions at the other two nonequivalent, "external" positions of the hydronium; and (iv) deuteration at the "bridge" position causes a ∼ 730 cm^{-1} red shift of the original central peak [curve (b)], whereas a deuteration at a tagged "external" position [the one with the highest frequency motion, in curve (c)] transforms the original triple-motif into a double one and promotes the appearance of a new dangling deuterium-mode at ω = 2070 cm^{-1}. Here again, the position of these two new D-features could be reasonably well predicted by a simple mass rescaling procedure.

In Figure 5, we present similar results for iodated clusters. The line shape for the fully protonated $IH\cdots OH_2(H_2O)_2$

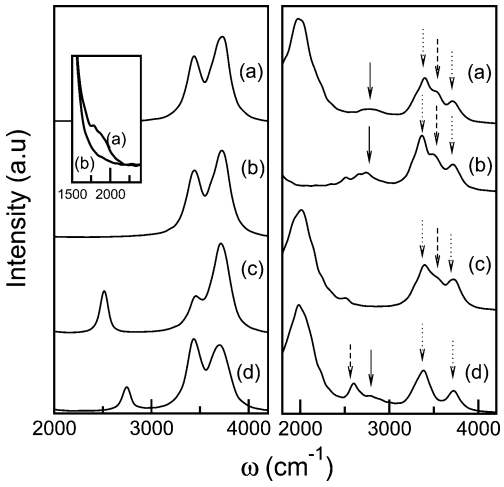

Figure 5. Stretching bands of RPMD infrared spectra of $HI\cdot(H_2O)_4$ clusters. Left panel: undissociated $IH\cdots OH_2(H_2O)_3$; right panel: dissociated $I^-\cdots(HOH_2)^+(H_2O)_2$. The letter code in both panels is the same: (a) fully protonated; (b) isotopomer with deuterium at "bridge" position; (c) isotopomer with deuterium at "external"-connective position; and (d) isotopomer with deuterium at "external"-dangling position. The inset in the left panel shows a 4 × zoomed image of curves (a and b).

moiety [curve (a) in the left-hand side panel] comprises two sub-bands and a dip at ∼3520 cm^{-1} that separates modes involving mostly connective protons from those with preferential participation of dangling protons. These two sub-bands are akin to the ones previously observed in small water clusters, such as the $[H_2O]_8$ case.[20] Unfortunately, at first glance, we failed to detect signals from modes involving the "bridge" proton which, based on the simple consideration of the magnitude of the stretching frequency in the isolated HI molecule, should appear at frequencies on the order of ∼2000 cm^{-1}. As such, deuteration at the "bridge" position did not promote any relevant modifications in the overall line shape [curves (a) and (b) look practically identical], except by the absence of a series of low-intensity humps localized at 1500−2000 cm^{-1} in the original spectrum, which are displayed in the 4 × zoomed profiles shown in the inset of the figure. This would confirm that contributions from the "bridge" local mode get washed out by much more intense contributions from the rest of the water dynamical modes. Curves (c and d) depict the modifications following deuterations at "external" connective and dangling positions, respectively. In the first case, one observes a new peak at ω = 2510 cm^{-1}, concomitant with a clear attenuation of the low-frequency original sub-band; conversely, the substitution at the "external"-dangling position shifts this new peak up to ω = 2740 cm^{-1}, whereas the attenuations are now registered in the high-frequency sub-band of the full protonated spectrum. The last analysis concerns the spectral signals of the $I^-\cdots(HOH_2)^+(H_2O)_2$ cluster (right-hand side panel). In curve (a), the list of the peaks corresponding to modes localized at the $(H_3O)^+$ ion includes: (i) a signal corresponding to motions of the "bridge" H, located at ω = 2100 cm^{-1}, significantly red-shifted and broadened, compared to the corresponding one in the ionic fluorinated cluster. The frequency shift is consistent with the 33.7 k_BT (HF) versus 18.2 k_BT (HI) reduction in the corresponding values of $\langle T^{\|}\rangle$ listed in Table 3c and with the larger extent of proton delocalization in HI also suggested by the corresponding $\langle c_i^2\rangle$ coefficients that we mentioned at the end of section IIIa; (ii) at $\omega \sim$ 2800 cm^{-1}, the spectrum presents a much lower intensity structure, which corresponds to stretching motions along the "external"-connective H of the cation (indicated by a solid arrow); and (iii) as one moves up in frequency, one observes a signal at $\omega \sim$ 3500 cm^{-1} comprising three sub-bands of decreasing amplitude. The central one, at ω = 3560 cm^{-1} (indicated by a dashed arrow), corresponds to the stretching mode localized at the dangling intramolecular bond in the hydronium, whereas the lateral ones can be ascribed to similar motions along connective and dangling bonds in water molecules (dotted arrows). The modifications operated upon selective deuteration are self-evident: the incorporations of the heavy isotope at the "bridge" [curve (b)] and "external"-connected [curve (c)] sites lead to the complete disappearances of the corresponding motifs in curve (a). We remark that the positions of the corresponding new D-peaks (not shown) are of difficult detection, since they overlap with the bending and "bridge" bands of curve (a). Finally, the deuteration at the "external"-dangling position shifts the peak down to 2560 cm^{-1}, a value of similar order to the one obtained by a direct mass rescaling.

IV. CONCLUDING REMARKS

The results presented in this paper provide new insights about the characteristics of hydrogen bonding at the vicinity of hydrogen halides, with different acid strengths, embedded in aqueous clusters at low temperatures. As such, the present work expands previous analyses, exploring aggregates with more complex structures beyond to those comprising pure water and simple anionic species. To accomplish that, we have implemented a molecular dynamics algorithm that combined the use of an MEVB Hamiltonian to achieve a proper description of proton transfer processes, along with a PI-RPMD scheme, to incorporate effects from nuclear quantum fluctuations on equilibrium and dynamical properties. In particular, we focused attention on clusters involving HF and HI, at the inceptions of their dissociative onsets, examining preferential solvation in structures that incorporates H and D at key connective locations.

In the isolated $FH\cdots OH_2$ dimer case, we found a clear propensity of the heavy isotope to lie along the weak acid−water hydrogen bond, compared to the alternative, dangling positions. This tendency, however, reverses for the $IH\cdots OH_2$ case. We found that the reasons for these differences can be traced back to the differences in the extents of spatial confinement prevailing at the two scenarios. For the $HF\cdots OH_2$ case, the thermodynamic stability is the result of a larger localization along both, parallel and perpendicular, directions with respect to the intermolecular H bond, compared to the

DOI: 10.1021/acs.jpca.6b06681
J. Phys. Chem. A 2016, 120, 7213−7224

one observed at the dangling OH intramolecular bond. Contrasting, for the IH···OH_2 case, it is the isotopomer with the light isotope lying along the connecting H-bond that is more stable. This change in stability is the result of sensible reductions of the quantum spatial confinements at the latter connecting position along parallel and, most notably, perpendicular directions. In this respect, this scenario resembles in part the one observed in clusters with even stronger HBs, such as the case of the $[H_2O{\cdots}H{\cdots}OH_2]^+$ Zundel complex, in which the most stable structures also correspond to those with the light isotope lying at the bridge position, and the key elements controlling the thermodynamic stability are the parallel projections of the corresponding kinetic energies. The latter feature contrasts with what is observed in other cluster and bulk environments,[20,24,76,82] in which the control is transferred to perpendicular projections. For the two acids, the extent of these thermodynamic positional propensities are modulated by the incorporation of increasing number of solvating water molecules; however, the qualitative trends remain valid, even after the onset of dissociation, in CIP solvation structures.

These predictions have also clear correlations with the overall characteristics of the lineshapes of the different stretching subbands of fully protonated clusters and selected deuterium substituted aggregates as well. We are confident that these theoretical predictions will be corroborated by direct experimental measurements opening interesting possibilities for assessing the strengths of the different H bonds along the intermolecular network via the analysis of the corresponding intensities and positions of mass-selected, spectroscopic signals of mixed clusters combining hydrogen halides, H_2O, and HDO.

AUTHOR INFORMATION

Corresponding Author

*E-mail: dhlaria@cnea.gov.ar. Tel: +54 (11)67727048. Fax: +54 (11)67727121.

Notes

The authors declare no competing financial interest.

ACKNOWLEDGMENTS

D.L. is a staff member of CONICET-ARGENTINA and acknowledges the support of this research from CONICET-Argentina (PIP 112-20110100464).

REFERENCES

(1) Dermota, T. E.; Zhong, Q.; Castleman, A. W., Jr. Ultrafast Dynamics in Cluster Systems. *Chem. Rev.* **2004**, *104*, 1861−1886.
(2) Young, R. M.; Neumark, D. M. Dynamics of Solvated Electrons in Clusters. *Chem. Rev.* **2012**, *112*, 5553−5577.
(3) Leopold, K. R. Hydrated Acid Clusters. *Annu. Rev. Phys. Chem.* **2011**, *62*, 327−349.
(4) Buch, V.; Bauerecker, S.; Devlin, J. P.; Buck, U.; Kazimirski, J. K. Solid Water Clusters in the Size Range of Tens-Thousands of H_2O: a Combined Computational/Spectroscopic Outlook. *Int. Rev. Phys. Chem.* **2004**, *23*, 375−433.
(5) Sanov, A.; Lineberger, W. C. Cluster Anions: Structure, Interactions, and Dynamics in the Sub-Nanoscale Regime. *Phys. Chem. Chem. Phys.* **2004**, *6*, 2018−2032.
(6) Headrick, J. M.; Diken, E. G.; Walters, R. S.; Hammer, N. I.; Christie, R. A.; Cui, J.; Myshakin, E. M.; Duncan, M. A.; Johnson, M. A.; Jordan, K. D. Spectral Signatures of Hydrated Proton Vibrations in Water Clusters. *Science* **2005**, *308*, 1765−1769.
(7) Guasco, T. L.; Johnson, M. A.; McCoy, A. B. Unraveling Anharmonic Effects in the Vibration Predissociation Spectra of $H_5O_2^+$ and its Deuterated Analogues. *J. Phys. Chem. A* **2011**, *115*, 5847−5858.
(8) Olesen, S. G.; Guasco, T. L.; Roscioli, J. R.; Johnson, M. A. Tuning the Intermolecular Proton Bond in the $H_5O_2^+$ 'Zundel Ion' Scaffold. *Chem. Phys. Lett.* **2011**, *509*, 89−95.
(9) Fournier, J. A.; Johnson, C. J.; Wolke, C. T.; Weddle, G. H.; Wolk, A. B.; Johnson, M. A. Vibrational Spectral Signature of the Proton Defect in the Three-Dimensional $H^+(H_2O)_{21}$ Cluster. *Science* **2014**, *344*, 1009−1012.
(10) Fournier, J. A.; Wolke, C. T.; Johnson, M. A.; Odbadrakh, T. T.; Jordan, K. D.; Kathmann, S. M.; Xantheas, S. S. Snapshots of Proton Accommodation at a Microscopic Water Surface: Understanding the Vibrational Spectral Signatures of the Charge Defect in Cryogenically Cooled $H^+(H_2O)n$ = 2 − 28 Clusters. *J. Phys. Chem. A* **2015**, *119*, 9425−9440.
(11) Thompson, W. H.; Hynes, J. T. Frequency Shifts in the Hydrogen-Bonded OH Stretch in Halide-Water Clusters. The Importance of Charge Transfer. *J. Am. Chem. Soc.* **2000**, *122*, 6278−6286.
(12) Rheinecker, J. L.; Bowman, J. M. The Calculated Infrared Spectrum of Cl^-H_2O Using a Full Dimensional Ab-initio Potential Surface and Dipole Moment Surface. *J. Chem. Phys.* **2006**, *124*, 131102.
(13) Ayotte, P.; Weddle, G. H.; Kim, J.; Johnson, M. A. Mass-Selected Matrix Isolation Infrared Spectroscopy of the $I^-{\cdot}(H_2O)_2$ Complex: Making and Breaking the Inter-Water Hydrogen-Bond. *Chem. Phys.* **1998**, *239*, 485−491.
(14) Baik, J.; Kim, H.; Majumdar, D.; Kim, K. S. Structures, Energetics, and Spectra of Fluoride-Water Clusters F(HO),n = 1−6: Ab Initio Study. *J. Chem. Phys.* **1999**, *110*, 9116−9127.
(15) Ayotte, P.; Nielsen, S. B.; Weddle, G. H.; Johnson, M. A.; Xantheas, S. S. Spectroscopic Observation of Ion-Induced Water Dimer Dissociation in the $X^-{\cdot}(H_2O)_2$ (X= F, Cl, Br, I) Clusters. *J. Phys. Chem. A* **1999**, *103*, 10665−10669.
(16) Ayotte, P.; Kelley, J. A.; Nielsen, S. B.; Johnson, M. A. Vibrational Spectroscopy of the F^-H_2O Complex Via Argon Predissociation: Photoinduced, Intracluster Proton Transfer? *Chem. Phys. Lett.* **2000**, *316*, 455−459.
(17) Horvath, S.; McCoy, A. B.; Roscioli, J. R.; Johnson, M. A. Vibrational Induced Proton Transfer in $F^-(H_2O)$ and $F^-(D_2O)$. *J. Phys. Chem. A* **2008**, *112*, 12337−12344.
(18) Robertson, W. H.; Johnson, M. A. Molecular Aspects of Halide Ion Hydration: The Cluster Approach. *Annu. Rev. Phys. Chem.* **2003**, *54*, 173−213.
(19) Ceriotti, M.; Fang, W.; Kusalik, P. G.; McKenzie, R. H.; Michaelides, A.; Morales, M. A.; Markland, T. E. Nuclear Quantum Effects in Water and Aqueous Systems: Experiment, Theory and Current Challenges. *Chem. Rev.* **2016**, *116*, 7529−7550.
(20) Videla, P. E.; Rossky, P. J.; Laria, D. Nuclear Quantum Effects on the Structure and the Dynamics of $[H_2O]_8$ at Low Temperatures. *J. Chem. Phys.* **2013**, *139*, 174315.
(21) Cheng, B.; Ceriotti, M. Direct Path Integral Estimators for Isotope Fractionation Ratios. *J. Chem. Phys.* **2014**, *141*, 244112.
(22) Marsalek, O.; Chen, P. Y.; Dupuis, R.; Benoit, M.; Méheut, M.; Bacić, Z.; Tuckerman, M. E. Efficient Calculation of Free Energy Differences Associated with Isotopic Substitution Using Path-Integral Molecular Dynamics. *J. Chem. Theory Comput.* **2014**, *10*, 1440−1453.
(23) Diken, E. G.; Shin, J.-W.; Price, E. A.; Johnson, M. A. Isotopic Fractionation and Zero-Point Effects in Anionic H-Bonded Complexes: a Comparison of the $I^-{\cdot}HDO$ and $F^-{\cdot}HDO$ Ion−Molecule Clusters. *Chem. Phys. Lett.* **2004**, *387*, 17−22.
(24) Videla, P. E.; Rossky, P. J.; Laria, D. Isotopic Preferential Solvation of I^- in Low-Temperature Water Nanoclusters. *J. Phys. Chem. B* **2015**, *119*, 11783−11790.
(25) McCunn, L. R.; Roscioli, J. R.; Elliott, B. M.; Johnson, M. A.; McCoy, A. B. Why Does Argon Bind to Deuterium? Isotope Effects and Structures of $Ar{\cdot}(H_5O)_5^+$ Complexes. *J. Phys. Chem. A* **2008**, *112*, 6074−6078.

DOI: 10.1021/acs.jpca.6b06681
J. Phys. Chem. A 2016, 120, 7213−7224

(26) Wilkins, D. M.; Manolopoulos, D. E.; Dang, L. X. Nuclear Quantum Effects in Water Exchange around Lithium and Fluoride Ions. *J. Chem. Phys.* **2015**, *142*, 064509.
(27) Warshel, A.; Weiss, R. M. An Empirical Valence Bond Approach for Comparing Reactions in Solutions and in Enzymes. *Ann. N. Y. Acad. Sci.* **1981**, *367*, 370−382.
(28) Ref 3 provides a comprehensive review of research work devoted to the analysis of $HX\cdot(H_2O)_n$ clusters.
(29) Walewski, L.; Forbert, H.; Marx, D. Quantum Induced Bond Centering in Microsolvated HCl: Solvent Separated versus Contact Ion Pairs. *J. Phys. Chem. Lett.* **2011**, *2*, 3069−3074.
(30) Forbert, H.; Masia, M.; Kaczmarek-Kedziera, A.; Nair, N. N.; Marx, D. Aggregation-induced Chemical Reactions: Acid Dissociation in Growing Water Clusters. *J. Am. Chem. Soc.* **2011**, *133*, 4062−4072.
(31) Masia, M.; Forbert, H.; Marx, D. Connecting Structure to Infrared Spectra of Molecular and Autodissociated HCl-Water Aggregates. *J. Phys. Chem. A* **2007**, *111*, 12181−12191.
(32) Gutberlet, A.; Schwaab, G.; Birer, Ö.; Masia, M.; Kaczmarek, A.; Forbert, H.; Havenith, M.; Marx, D. Aggregation-Induced Dissociation of $HCl(H_2O)_4$ Below 1 K: the Smallest Droplet of Acid. *Science* **2009**, *324*, 1545−1548.
(33) Lin, W.; Paesani, F. Infrared Spectra of $HCl(H_2O)_n$ Clusters from Semiempirical Born-Oppenheimer Molecular Dynamics Simulations. *J. Phys. Chem. A* **2015**, *119*, 4450−4456.
(34) Ndongmouo, U. F. T.; Lee, M. S.; Rousseau, R.; Baletto, F.; Scandolo, S. Finite-Temperature Effects on the Stability and Infrared Spectra of $HCl(H_2O)_6$ Clusters. *J. Phys. Chem. A* **2007**, *111*, 12810−12815.
(35) Mancini, J. S.; Bowman, J. M. Effects of Zero-Point Delocalization on the Vibrational Frequencies of Mixed HCl and Water Clusters. *J. Phys. Chem. Lett.* **2014**, *5*, 2247−2253.
(36) Weimann, M.; Fárník, M.; Suhm, M. A. A First Glimpse at the Acidic Proton Vibrations in HCl-water Clusters via Supersonic Jet FTIR Spectroscopy. *Phys. Chem. Chem. Phys.* **2002**, *4*, 3933−3937.
(37) Huneycutt, A. J.; Stickland, R. J.; Hellberg, F.; Saykally, R. J. Infrared Cavity Ringdown Spectroscopy of Acid-Water Clusters: HCl-H_2O, DCl-D_2O and DCl-$(D_2O)_2$. *J. Chem. Phys.* **2003**, *118*, 1221−1229.
(38) Fárník, M.; Weimann, M.; Suhm, M. A Comparative Jet Fourier Transform Infrared Study of Small HCL and HBr-Solvent Complexes. *J. Chem. Phys.* **2003**, *118*, 10120−10136.
(39) Skvortsov, D.; Lee, S. J.; Vilesov, M. Y.; Choi, M. Y. Hydrated HCl Clusters, $HCl(H_2O)_{1-3}$ in Helium Nanodroplets: Studies of Free OH Vibrational Stretching Modes. *J. Phys. Chem. A* **2009**, *113*, 7360−7365.
(40) Craig, I. R.; Manolopoulos, D. E. Quantum Statistics and Classical Mechanics: Real Time Correlation Functions from Ring Polymer Molecular Dynamics. *J. Chem. Phys.* **2004**, *121*, 3368−3373.
(41) Habershon, S.; Manolopoulos, D. E.; Markland, T. E.; Miller, T. F., III Ring-Polymer Molecular Dynamics: Quantum Effects in Chemical Dynamics from Classical Trajectories in an Extended Phase Space. *Annu. Rev. Phys. Chem.* **2013**, *64*, 387.
(42) Feynman, R. P.; Hibbs, A. R. *Quantum Mechanics and Path Integrals*; McGraw-Hill: New York, 1965.
(43) Voth, G. A. Computer Simulation of Proton Solvation and Transport in Aqueous and Biomolecular systems. *Acc. Chem. Res.* **2006**, *39*, 143−150.
(44) Čuma, M.; Schmitt, U. W.; Voth, G. A. A Multi-State Empirical Valence Bond Model for Acid-Base Chemistry in Aqueous Solutions. *Chem. Phys.* **2000**, *258*, 187−199.
(45) Čuma, M.; Schmitt, U. W.; Voth, G. A. A Multi-State Empirical Valence Bond Model for Weak Acid Dissociation in Aqueous Solution. *J. Phys. Chem. A* **2001**, *105*, 2814−2823.
(46) Wang, F.; Izvekov, S.; Voth, G. A. Unusual Amphiphilic Association of Hydrated Protons in Strong Acid Solution. *J. Am. Chem. Soc.* **2008**, *130*, 3120−3126.
(47) Vuilleumier, R.; Borgis, D. *Classical and Quantum Dynamics in Condensed Phase Simulations*; Berne, B. J., Ciccotti, G., Coker, D. F., Eds.; World Scientific: Singapore, 1998; Chapter 30.
(48) Joutsuka, T.; Ando, K. Hydration Structure in Dilute Hydrofluoric Acid. *J. Phys. Chem. A* **2011**, *115*, 671−677.
(49) Videla, P. E.; Rossky, P. J.; Laria, D. Isotopic Effects on Tunneling Motions in the Water Trimer. *J. Chem. Phys.* **2016**, *144*, 061101.
(50) Maupin, C. M.; Wong, K. F.; Soudackov, A. V.; Kim, S.; Voth, G. A. A Multistate Empirical Valence Bond Description of Protonable Amino Acids. *J. Phys. Chem. A* **2006**, *110*, 631−639.
(51) Park, K.; Lin, W.; Paesani, F. A Refined MS-EVB Model for Proton Transport in Aqueous Environments. *J. Phys. Chem. B* **2012**, *116*, 343−352.
(52) Perera, L.; Berkowitz, M. L. Many Body Effects in Molecular Dynamics Simulations of $Na^+(H2O)_n$ and $Cl^-(H2O)_n$ Clusters. *J. Chem. Phys.* **1991**, *95*, 1954−1963.
(53) Carignano, M. A.; Karlström, G.; Linse, P. Polarizable Ions in Polarizable Water: A Molecular Dynamics Study. *J. Phys. Chem. B* **1997**, *101*, 1142−1147.
(54) Stuart, S. J.; Berne, B. J. Effects of Polarizability on the Hydration of the Chloride Ion. *J. Phys. Chem.* **1996**, *100*, 11934−11943.
(55) Dang, L. X. Characterization of Water Octamer, Nanomer, Decamer, and Iodide Water Interactions using Molecular Dynamics Techniques. *J. Chem. Phys.* **1999**, *110*, 1526−1532.
(56) Yoo, S.; Lei, Y. A.; Zeng, X. C. Effect of Polarizability of Halide Anions on the Ionic Solvation in Water Clusters. *J. Chem. Phys.* **2003**, *119*, 6083−6091.
(57) Frisch, M. J.; Trucks, G. W.; Schlegel, H. B.; Scuseria, G. E.; Robb, M. A.; Cheeseman, J. R.; Montgomery, J. A., Jr.; Vreven, T.; Kudin, K. N.; Burant, J. C. et al. *Gaussian 03*, revision C.02.; Gaussian, Inc.: Wallingford, CT, 2004.
(58) Peterson, K. A.; Shepler, B. C.; Figgen, D.; Stoll, H. On the Spectroscopic and Thermochemical Properties of ClO, BrO, IO, and their Anions. *J. Phys. Chem. A* **2006**, *110*, 13877−13883.
(59) Maroulis, G. Is the Dipole Polarizability of Hydrogen Iodide Accurately Known? *Chem. Phys. Lett.* **2000**, *318*, 181−189.
(60) Archontis, G.; Leontidis, E.; Andreou, G. Attraction of Iodide Ions by the Free Water Surface, Revealed by Simulations with a Polarizable Force Field based on Drude Oscillations. *J. Phys. Chem. B* **2005**, *109*, 17957−17966.
(61) Tuckerman, M. E. *Statistical Mechanics: Theory and Molecular Simulation*; Oxford University Press, 2010; Chapter 10.
(62) Feynman, R. P. Forces in Molecules. *Phys. Rev.* **1939**, *56*, 340−343.
(63) Habershon, S.; Fanourgakis, G. S.; Manolopoulos, D. E. Comparison of Path Integral Molecular Dynamics Methods for the Infrared Absorption Spectrum of Liquid Water. *J. Chem. Phys.* **2008**, *129*, 074501.
(64) Tuckerman, M.; Berne, B. J.; Martyna, G. J. Reversible Multiple Time Scale Molecular Dynamics. *J. Chem. Phys.* **1992**, *97*, 1990−2001.
(65) Ceriotti, M.; Parrinello, M.; Markland, T. E.; Manolopoulos, D. E. Efficient Stochastic Thermostatting of Path Integral Molecular Dynamics. *J. Chem. Phys.* **2010**, *133*, 124104.
(66) Re, S. Enhanced Stability of Non-Proton-Transferred Clusters of Hydrated Hydrogen Fluoride $HF(H_2O)_n$ (n = 1 − 7): a Molecular Orbital Study. *J. Phys. Chem. A* **2001**, *105*, 9725−9735.
(67) Odde, S.; Mhin, B. J.; Lee, S.; Lee, H. M.; Kim, K. S. Dissociation Chemistry of Hydrogen Halides in Water. *J. Chem. Phys.* **2004**, *120*, 9524−9535.
(68) Odde, S.; Mhin, B. J.; Lee, K. W.; Lee, H. M.; Tarakeshwar, P.; Kim, K. S. Hydration and Dissociation of Hydrogen Fluoric Acid (HF). *J. Phys. Chem. A* **2006**, *110*, 7918−7924.
(69) Xie, Z. Z.; Ong, Y. S.; Kuo, J. L. On the Effects of Basis-Set in Studying the Hydration and Dissociation of HF in Cubic $HF(H_2O)_7$ Clusters. *Chem. Phys. Lett.* **2008**, *453*, 13−17.
(70) Cabaleiro-Lago, E. M.; Hermida-Ramón, J. M.; Rodriguez-Otero, J. Computational Study of the Dissociation of H-X Acids (X = F, Cl, Br, I) in Water Clusters. *J. Chem. Phys.* **2002**, *117*, 3160−3168.
(71) Elena, A. M.; Meloni, S.; Ciccotti, G. Equilibrium and Rate Constants, and Reaction Mechanism of the HF Dissociation in the

DOI: 10.1021/acs.jpca.6b06681
J. Phys. Chem. A 2016, 120, 7213−7224

$HF(H_2O)_7$ Cluster by Ab Initio Rare Event Simulation. *J. Phys. Chem. A* **2013**, *117*, 13039−13050.
(72) Ando, K.; Hynes, J. T. HF Acid Dissociation in Water: the First Step. *Faraday Discuss.* **1995**, *102*, 435−441.
(73) Ando, K.; Hynes, J. T. Molecular Mechanism of HF Acid Ionization in Water: an Electronic Structure-Monte Carlo Study. *J. Phys. Chem. A* **1999**, *103*, 10398−10408.
(74) Vaníček, J.; Miller, W. H. Efficient Estimators for Quantum Instanton Evaluation of the Kinetic Isotope Effects: Application to the Intramolecular Hydrogen Transfer in Pentadiene. *J. Chem. Phys.* **2007**, *127*, 114309.
(75) Ceriotti, M.; Markland, T. E. Efficient Methods and Practical Guidelines for Simulating Isotope Effects. *J. Chem. Phys.* **2013**, *138*, 014112.
(76) Liu, J.; Andino, R. S.; Miller, C. M.; Chen, X.; Wilkins, D. M.; Ceriotti, M.; Manolopoulos, D. E. A Surface-Specific Isotope Effect in Mixture of Light and Heavy Water. *J. Phys. Chem. C* **2013**, *117*, 2944−2951.
(77) Videla, P. E.; Rossky, P. J.; Laria, D. Surface Isotope Segregation as a Probe of Temperature in Water Nanoclusters. *J. Phys. Chem. Lett.* **2014**, *5*, 2375−2379.
(78) Pinilla, C.; Blanchard, M.; Balan, E.; Ferlat, G.; Vuilleumier, R.; Mauri, F. Equilibrium Fractionation of H and O Isotopes in Water from Path Integral Molecular Dynamics. *Geochim. Cosmochim. Acta* **2014**, *135*, 203−216.
(79) See, for example, Vuilleumier, R. Transport et Spectroscopie du Proton en Solution Aqueuse: une Étude de Dynamique Moléculaire. Ph.D. Thesis, University of Paris VI, 1998.
(80) Witt, A.; Ivanov, S. D.; Shiga, M.; Forbert, H.; Marx, D. On the Applicability of Centroids and Ring Polymer Path Integral Molecular Dynamics for Vibrational Spectroscopy. *J. Chem. Phys.* **2009**, *130*, 194510.
(81) Rossi, M.; Ceriotti, M.; Manolopoulos, D. E. How to Remove the Spurious Resonances from Ring Polymer Dynamics. *J. Chem. Phys.* **2014**, *140*, 234116.
(82) Markland, T. E.; Berne, B. J. Unraveling Quantum Mechanical Effects in Water using Isotopic Fractionation. *Proc. Natl. Acad. Sci. U. S. A.* **2012**, *109*, 7988−7991.

DOI: 10.1021/acs.jpca.6b06681
J. Phys. Chem. A 2016, 120, 7213−7224